JOURNAL OF CATALYSIS **163,** 63–76 (1996)
ARTICLE NO. 0305

Surface-Enhanced Raman Spectroscopy as an *in Situ* Real-Time Probe of Catalytic Mechanisms at High Gas Pressures:

The CO–NO Reaction on Platinum and Palladium

Christopher T. Williams,* Anish A. Tolia,* Ho Yeung H. Chan,* Christos G. Takoudis,* and Michael J. Weaver†

**School of Chemical Engineering and †Department of Chemistry, Purdue University, West Lafayette, Indiana 47907*

Received December 18, 1995; revised April 25, 1996; accepted April 30, 1996

Surface-enhanced Raman spectroscopy (SERS), combined with simultaneous mass spectrometric measurements, has been utilized to probe the reactive nature of surface species present during the reduction of NO by CO on Pt and Pd. As in our earlier studies, the SERS-active transition-metal surfaces are prepared by electrodepositing ultrathin films onto electrochemically roughened gold. These surfaces display remarkably robust SERS activity, enabling intense Raman spectra to be obtained over a range of reactant pressures (here up to 1 atm) and at temperatures up to at least 400°C. During nitric oxide adsorption at 1 atm on Pt, both terminal (240 and 470 cm^{-1}) and bridged (325 cm^{-1}) states of molecular NO were detected at lower temperatures (25–200°C), with some dissociation occurring at higher (ca 250°C) temperatures as evidenced by the presence of atomic nitrogen (295 cm^{-1}). Similarly, a bridged NO species (310 cm^{-1}) was observed on Pd under similar conditions, with dissociation detected in the form of atomic nitrogen (285 cm^{-1}) and surface oxide (450 and 665 cm^{-1}). Co-dosing of reactants on platinum produced a surface dominated by NO and CO (470 and 2080 cm^{-1}), whereas the former was adsorbed preferentially on Pd. Simultaneous SERS/MS measurements were performed during reaction of an equimolar reactant mixture at 1 atm of total pressure over both metals. Both CO_2 and N_2O were formed during reaction on Pt, with onset of detectable product formation correlating with depletion of adsorbed CO and NO, respectively. In contrast, CO_2 was the only product detected over Pd, with the depletion of surface oxygen suggesting that NO dissociation may be rate limiting at higher temperatures (ca 300°C). The extent of dissociation on these surfaces is compared and contrasted, with particular emphasis placed on its role in determining reaction selectivity. Furthermore, the overall behavior of these catalysts is compared with our former observations regarding this reduction process on rhodium.

INTRODUCTION

The reduction of NO by CO over supported transition metals has been investigated extensively due to automobile emission standards which have been instituted over the years. The possibility of three products (CO_2, N_2O, and N_2) raises issues regarding selectivity of different catalysts and the mechanisms by which these reactions take place. As a result, a large amount of effort has been expended on the study of this reaction over platinum, palladium and rhodium.

The ability of these catalysts to dissociate adsorbed NO appears to lie at the heart of the issues of selectivity and overall rates. While studies involving NO adsorption under ultrahigh vacuum (UHV) conditions on both single crystal and polycrystalline Pt (1–11) and Pd (12–22) have revealed similar yet modest levels of NO dissociation, Rh is significantly more active in this regard (see Ref. (23) and cited literature therein). In the case of all three catalysts, more highly stepped surfaces appear to facilitate NO dissociation (20, 24). The link between NO dissociation capability and overall reaction rates is supported, for example, by investigations of NO reduction over single crystal Pt surfaces (25–34). The Pt(111) surface was found to be practically inert, while stepped Pt(410) was the most active face, probably because of its greater ability to dissociate NO. However, there is much controversy in the literature over whether NO dissociation (25, 26, 34–36) or a bimolecular surface reaction between adsorbed NO and CO (37–42) is the rate-determining step. Related to these issues is the selectivity of these materials towards CO_2 and/or N_2O formation. In our recent study of the CO–NO reaction at atmospheric pressure on Rh, CO_2, and N_2 were observed to be the only major products (23). In contrast, both N_2O and CO_2 have been observed during reaction on supported palladium (42, 43) and platinum (35). However, other investigations involving Pt (34, 37) and Pd (44) catalysts have reported CO_2 and N_2 as the major products.

The contradictory nature of many of these findings underscores the need for techniques that are able to examine catalyst surfaces *in situ* under reaction conditions. With

0021-9517/96 $18.00

its superior surface sensitivity, especially at high gas pressures, surface enhanced Raman spectroscopy (SERS) can offer a unique view of the surface species present under technologically relevant conditions. We have demonstrated, through earlier studies in our laboratory, that the SERS effect can be extended to transition metals, including Pt and Pd, by depositing them as thin films on roughened gold electrodes (45, 46). Such films have been shown to exhibit stable as well as intense SERS activity in the gas phase even at elevated temperatures (23, 47–52). As a result, the wide frequency range along with the real-time capability afforded by SERS may be exploited to yield information regarding gas–surface interactions for reactive systems at high pressures that are not easily accessible through more conventional methods. By correlating the behavior of surface species with gas-phase reaction products as monitored by simultaneous mass spectrometric (MS) analysis, information can be obtained regarding the possible role of the adsorbed molecules in the reaction pathway (23).

We have recently reported results of a detailed examination along these lines of the CO–NO reaction on Rh thin films, utilizing this approach to elucidate the role of the adsorbed species (atomic nitrogen and CO) in the overall reaction (23). The study described herein for the same reaction on Pt and Pd films extends this effort to a pair of surfaces that, although being effective catalysts, dissociate NO to a markedly smaller extent than on Rh. This forms part of a continuing effort in our group to employ SERS combined with simultaneous mass spectrometric measurements of the gas phase to probe heterogeneous catalytic reactions. In order to gain more perspective on the CO–NO reaction, intercomparisons are made between this process over Pt, Pd, and Rh. In addition, we present infrared spectral data which provide an independent check on, as well as a complement to, the SERS results.

EXPERIMENTAL

The SERS-active surfaces were prepared utilizing 6 mm diameter discs cut out of 0.1 mm thick gold foil (Johnson Matthey), and polished using 0.3 μm alumina powder. They were then placed into an electrode holder that exposed Ca 7 mm^2 of the surface and subjected to 25 oxidation–reduction cycles from -0.3 to 1.2 V versus SCE at 0.5 V s^{-1} in 0.1 *M* KCl to produce the surface roughness necessary for Raman enhancement (53). The surface was rinsed thoroughly with deionized water and subsequently transferred to another cell for electrochemical deposition of the Pt or Pd overlayer. Platinum was deposited from a 0.3 m*M* solution of H_2PtCl_6 in 0.1 *M* H_2SO_4 at 0.15 V versus SCE, while palladium was deposited from a 0.5 m*M* solution of $PdCl_2$ in 0.1 *M* $HClO_4$ at 0.1 V versus SCE. In both instances the cathodic charge was monitored and controlled in order to limit the deposition to the desired film thickness, usually less than five equivalent monolayers (45, 46).

The reactor utilized for the SERS experiments consists of a 100 cm^3 volume six-way cross, equipped with a turbomolecular pump (Balzers TPH 060) yielding a base pressure of 2×10^{-6} Torr (23). A combination of needle, gate, and butterfly valves allows operation of the reactor at pressures ranging from 10^{-3} to 760 Torr. The pressure over the entire range is measured using a combination of Pirani and cold-cathode gauges, controlled by a Balzers TPG 252 pressure controller. One of the reactor arms contains an optical viewport, over which the specimen is mounted on a stainless steel cylindrical sample holder which can be heated to 500°C. Inside the sample holder, a solid piece of stainless steel is surrounded by a coil of thin nichrome wire to provide resistive heating. Through the center of this heater is a K-type thermocouple which leads to an programmable temperature controller (Omega CN2041). Laser excitation is provided by a Kr^+ laser at 647.1 nm (Spectra Physics) and scattered light is collected by a three-stage spectrometer (SPEX Triplemate). The spectrometer is equipped with a liquid nitrogen-cooled CCD (Photometrics), allowing acquisition of real-time spectral sequences typically even on a seconds time scale with a good signal-to-noise ratio. Gas-phase compositions are measured with a mass spectrometer (VG Instruments SX 200) interfaced with a Zenith Data Systems Z-248 computer. The gas is leaked into the mass spectrometer from a differentially pumped capillary line that samples directly from the reactor.

Infrared reflection–absorption spectroscopic (IRAS) measurements were carried out in a Nicolet 800 FTIR spectrometer equipped with a MCT detector. The reactor used is a small volume (5 cm^3) chamber equipped with KBr windows which could be evacuated to 0.1 Torr (Spectra Tech). The samples were heated using a heating element identical to that described for the SERS reactor (*vide supra*). Gases were mixed through a manifold and flow rates were measured with a bubble flow meter. Spectra were collected using near-grazing angle optics (Pike Technologies) in a single-reflectance mode. Spectral features arising from surface species were differentiated from their gas-phase counterparts by subtracting data obtained with *s*- and *p*-polarized light. Each spectrum was collected utilizing 1500 scans and 4 cm^{-1} resolution, and proportioned to background spectra obtained prior to the reactant dosage.

Both reactors behave as a well-mixed CSTR, as shown by the transient response of the reactor composition with changes in gas flow conditions. The reactants are introduced into the reactor through a manifold that allows mixing of up to four inlet gases and flow rates are measured with a bubble flow meter. All reactants used in this study were of ultra-high purity and obtained from Matheson and Airco gases.

RESULTS

Platinum Films

Initial spectral examination of newly prepared platinum thin films occasionally revealed SERS features at 330 and 260 cm^{-1} associated with Pt–Cl and Au–Cl species remaining from the deposition process. In such cases, the samples were pretreated in 100 cm^3 min^{-1} H_2 at 150°C for ca 10 min, which resulted in a clean background in the 200–1000 cm^{-1} region. Nonetheless, broad bands resulting from surface carbonaceous impurities were commonly discerned in the 1300–1600 cm^{-1} region, removal of which required prior high-temperature oxidation. This, however, resulted in severe disruption of the film with consequent partial loss of SERS activity and was therefore not used here as part of the pretreatment procedure.

The temperature-dependent adsorption of the individual reactants was examined with SERS prior to *in situ* real-time probing of the surface under reaction conditions. Figure 1 shows a typical temperature-dependent spectral sequence for a Pt film exposed to 100 cm^3 min^{-1} of NO at 1 atm. The two spectral regions shown in Figs. 1A and B (ca 200–800 cm^{-1} and 1700–2400 cm^{-1}, respectively) were obtained separately in order to achieve satisfactory frequency resolution with the CCD detector employed. Prior to adsorption of the reactant, the reactor was evacuated to ca 10^{-5} Torr to purge the system of gas-phase contaminants. Following NO dosage, the sample was heated in a stepwise periodic fashion, allowing sufficient time at each temperature (ca 3 min) for the spectra to attain time-independent behavior.

Several features are apparent upon dosing of NO at room temperature (bottom spectrum). Two sharp peaks are observed at 240 and 325 cm^{-1} along with two broader bands at ca 470 and 610 cm^{-1} (Fig. 1A). Raman bands at 2180 and 2250 cm^{-1} are also evident in the corresponding higher frequency spectra (Fig. 1B). The remaining spectra in the sequence, stacked in an upward direction, show the results of heating the sample to the temperatures indicated. Upon heating to 150°C, the most noticeable change is the marked intensity increase in the 2250 cm^{-1} feature (Fig. 1B) which is accompanied by milder intensity enhancements in the 240, 470, and 610 cm^{-1} bands (Fig. 1A). At the same time, the 325 cm^{-1} band is attenuated. Raising the temperature to 200°C results in the disappearance of the 2250 cm^{-1} peak and attenuation of the remaining features, along with the appearance of a weak band at 295 cm^{-1}. Further heating to 300°C caused attenuation of the remaining bands, with final removal by 350°C.

Assignment of these features to specific vibrations is not entirely straightforward and is discussed below. In order to help the reader's appreciation of the spectral results, however, we mention in advance our tentative assignment of the 240 and 470 cm^{-1} bands to Pt–NO stretching and Pt–N–O bending modes, respectively, of NO adsorbed on atop (i.e., terminal) sites. The 325 cm^{-1} feature is attributed to the Pt–NO stretch of NO adsorbed on bridge sites.

The adsorption of CO on platinum at room temperature resulted in spectra as shown in Figs. 2A, B. Two features can

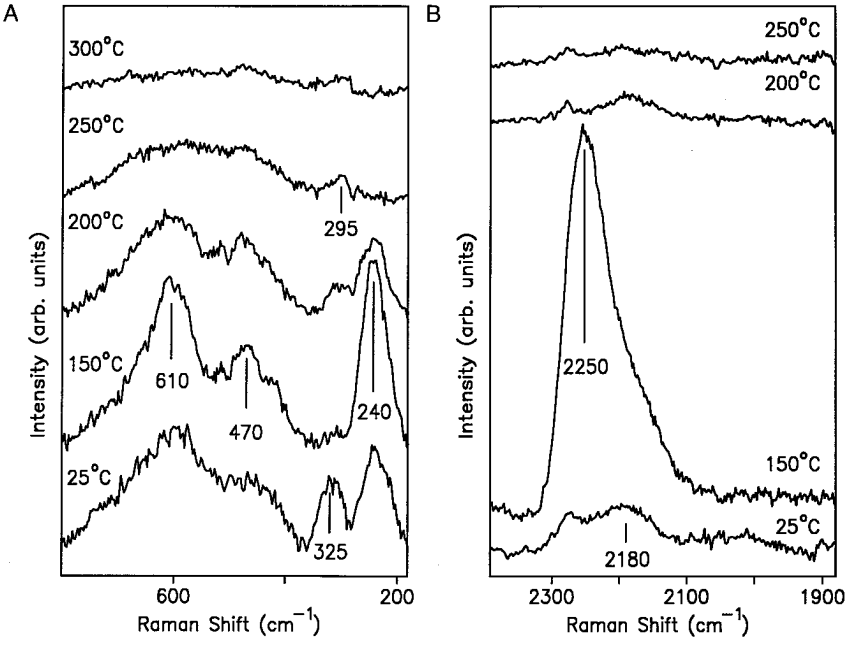

FIG. 1. Temperature-dependent SER spectra for a Pt surface exposed to 100 cm^3 min^{-1} NO at 1 atm: (A) Low frequency spectra obtained with 20 s integration time; (B) High frequency spectra obtained with 60 s integration time.

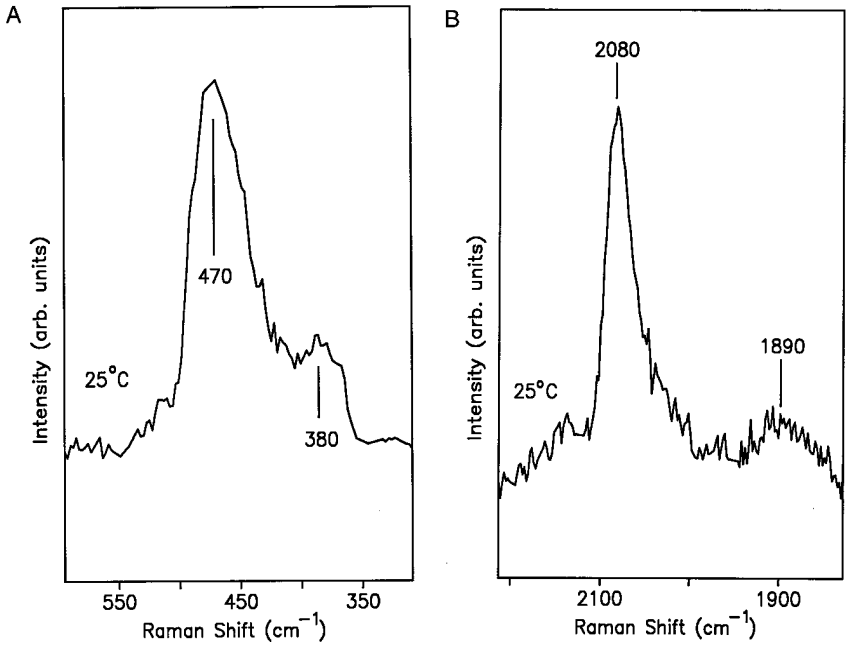

FIG. 2. SER spectrum of a Pt surface exposed to 100 cm^3 min^{-1} of CO at 1 atm: (A) Low frequency spectra obtained with 20 s integraton time; (B) High frequency spectra.

be seen at 470 and 380 cm^{-1} in the low-frequency region (Fig. 2A) accompanied by bands at 2080 and 1890 cm^{-1} in the higher frequency spectra (Fig. 2B). Although heating the sample in CO resulted in deteriorating signal quality due to loss of SERS activity, the bands appear to remain on the surface until at least 350°C. As in the SERS study of CO and NO adsorption on Pt, Rh, and Ru by Wilke *et al.* (47), the 470 and 2080 cm^{-1} peaks are assigned to the Pt–CO and C–O stretches of terminally adsorbed (i.e., atop) CO, while the 380 and 1890 cm^{-1} bands are similarly attributed to CO bound to twofold bridging sites. A basis for these assignments is that similar frequencies for both the Pt–CO and C–O stretches have also been reported in FTIR (54) and EELS (55) studies of CO adsorption on Pt surfaces in UHV.

The form of the C–O and Pt–CO stretching bands for adsorbed CO was also examined for various $^{13}CO/^{12}CO$ isotopic mixtures in addition to dosing with ^{12}CO as noted above. These experiments were prompted primarily by the insight that can be obtained into the extent of adsorbate dipole–dipole coupling in this manner, and hence the effective local CO coverage present on the Pt surface (56). Specifically, high local (i.e., microscopic) coverages of CO will yield substantial dipole coupling for the C–O stretching (ν_{CO}) vibration. This is signaled in part by markedly higher intensities of the higher-frequency (ν_{CO}) partner than expected on the basis of the relative $^{12}CO/^{13}CO$ coverages. Typical data obtained during such an experiment, involving an equimolar $^{12}CO/^{13}CO$ mixture, is shown in Fig. 3. The C–O stretch region shows a pair of peaks displaying the marked "intensity transfer" expected for strong dipole–dipole coupling: an intense high-frequency (ν_{CO}) feature (2060 cm^{-1}) and a markedly weaker lower frequency (2010 cm^{-1}) band. As observed in Fig. 2B, the broad feature

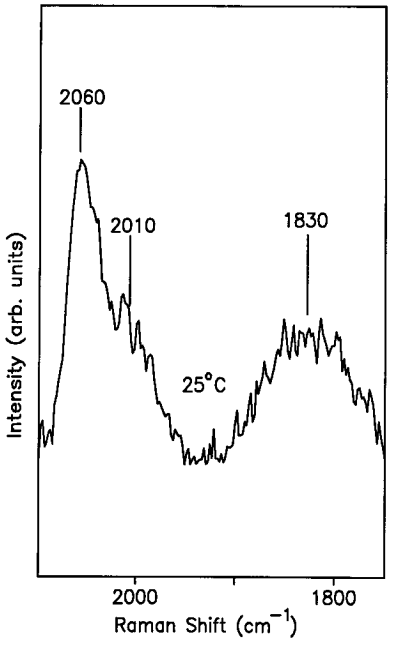

FIG. 3. High-frequency SER spectra obtained with 60 s integration time of a Pt surface exposed to a mixture of 50% ^{12}CO and 50% ^{13}CO.

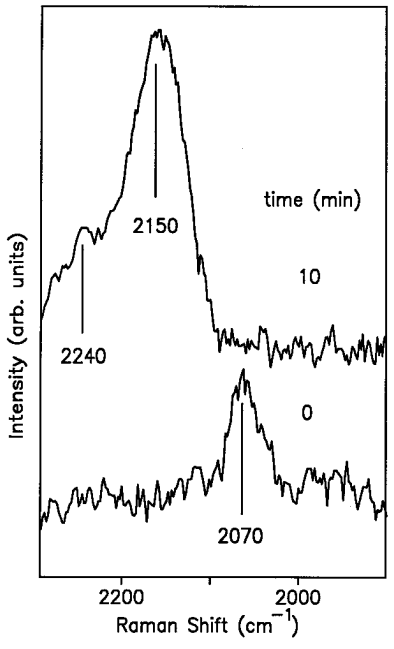

FIG. 4. High-frequency region of SER spectra obtained before and after dosing NO on a CO-saturated surface.

centered at 1830 cm^{-1} is indicative of CO adsorbed at twofold bridging sites. This strong coupling effect confirms the presence of a high local coverage of CO, an assertion which is supported by IRAS experiments discussed below.

As demonstrated in our earlier study of the CO–NO reaction on Rh (23), real-time SERS can be effectively utilized to probe competitive adsorption of the two reactants, which in turn can provide insight into reaction mechanisms. Since both NO and CO yield strong spectral features upon adsorption, experiments involving sequential reactant dosing were performed to assess the competitive nature of this process. In each case, the sample was initially exposed to 100 $cm^3\ min^{-1}$ of one reactant at 25°C until the spectral features attained a constant intensity. The chamber was subsequently evacuated to 10^{-5} Torr and then filled with 100 $cm^3\ min^{-1}$ of the other reactant, which essentially instantaneously (ca < 1 s) exposed the sample to 1 atm of pure gas.

Typical results along these lines for a CO-predosed surface exposed subsequently to NO are shown in Fig. 4. Just prior to NO addition, at t = 0 s (bottom spectra), a strong feature was observed at 2070 cm^{-1}, indicative of CO adsorbed at terminal sites. After ca 10 min exposure to NO (top spectra), however, these features are no longer evident and strong 2150 and 2240 cm^{-1} bands have developed. The loss of the CO spectral features indicates clearly that NO is able to displace CO under these conditions. The converse experiment, involving CO dosing onto a NO-predosed surface, yielded no detectable CO-induced changes in the NO spectral features, showing that the reverse process is not facile. Attempts were also made to conduct similar experiments at elevated temperatures. However, heating the Pt film to temperatures greater than 150°C in vacuum (i.e., prior to reactant dosing) often resulted in an irreversible loss of SERS activity, making it difficult to obtain reproducible data under these conditions.

In order to obtain information linking the overall temperature-dependent surface speciation with the catalytic rates, the reaction for various CO and NO ratios on the platinum films was probed by mass spectrometry (MS) simultaneously with SERS. The general procedure followed for these experiments was similar to the one used in our recent study of the CO–NO reaction on Rh (23). The masses monitored were 28 (CO and/or N_2), 30 (NO), and 44 (CO_2 and/or N_2O), with data acquired continuously and recorded every 5 s. Following exposure to each reactant mixture, samples were heated in a stepwise periodic fashion, waiting at each temperature for a time-independent response to be reached (ca 3 min) before spectra were acquired.

Figures 5A–C show such simultaneously obtained temperature-dependent SERS (A, B) and MS measurements (C) for a Pt surface exposed to an equimolar mixture of NO and CO, specifically 50 $cm^3\ min^{-1}$ of each at 1 atm and 25°C. The ambient-temperature SER spectra show features arising from both CO and NO, with low-frequency bands at 240, 325, 470, and 640 cm^{-1} (Fig. 5A) and higher frequency features at 2080, 2160, and 2230 cm^{-1} (Fig. 5B). Upon heating to 125°C, the only noticeable change is the attenuation of the 640 cm^{-1} feature. Heating further to 200°C, however, diminishes the intensities of the 325, 470, and 2080 cm^{-1} bands, the last indicating removal of adsorbed CO. Severe attenuation of all the SERS features is seen above 250°C, although traces of the 2230, 2160, and 470 cm^{-1} features still remain even at 350°C. The corresponding gas-phase composition, as gleaned from the mass 44 intensity, is shown in Fig. 5C. Raising the temperature to 200°C and beyond is seen to trigger the onset of detectable reaction to form CO_2 and/or N_2O (*vide infra*), with the signature mass 44 intensity exhibiting a monotonic increase with further temperature elevation, albeit somewhat muted above 250°C.

Mass spectrometric measurements under equimolar reactant conditions using the ^{13}CO isotope were also obtained in order to separate the contributions to the mass 44 intensity arising from the two possible (CO_2 and N_2O) products. Masses 29 (^{13}CO), 30 (NO), 44 (N_2O), and 45 ($^{13}CO_2$) were monitored together at 5-s intervals as the temperature was raised in a stepwise fashion. Figure 6 shows a plot of the intensities of masses 44 and 45 for an equimolar mixture (10 $cm^3\ min^{-1}$ each) of CO and NO. The results indicate detectable formation of both $^{13}CO_2$ (mass 45) above 200°C and N_2O (mass 44) above 300°C, although the intensity of the latter is markedly smaller, suggesting that the major product is CO_2 under these conditions.

The reaction between CO and NO was also examined in an identical fashion to Fig. 5, but now utilizing mixtures

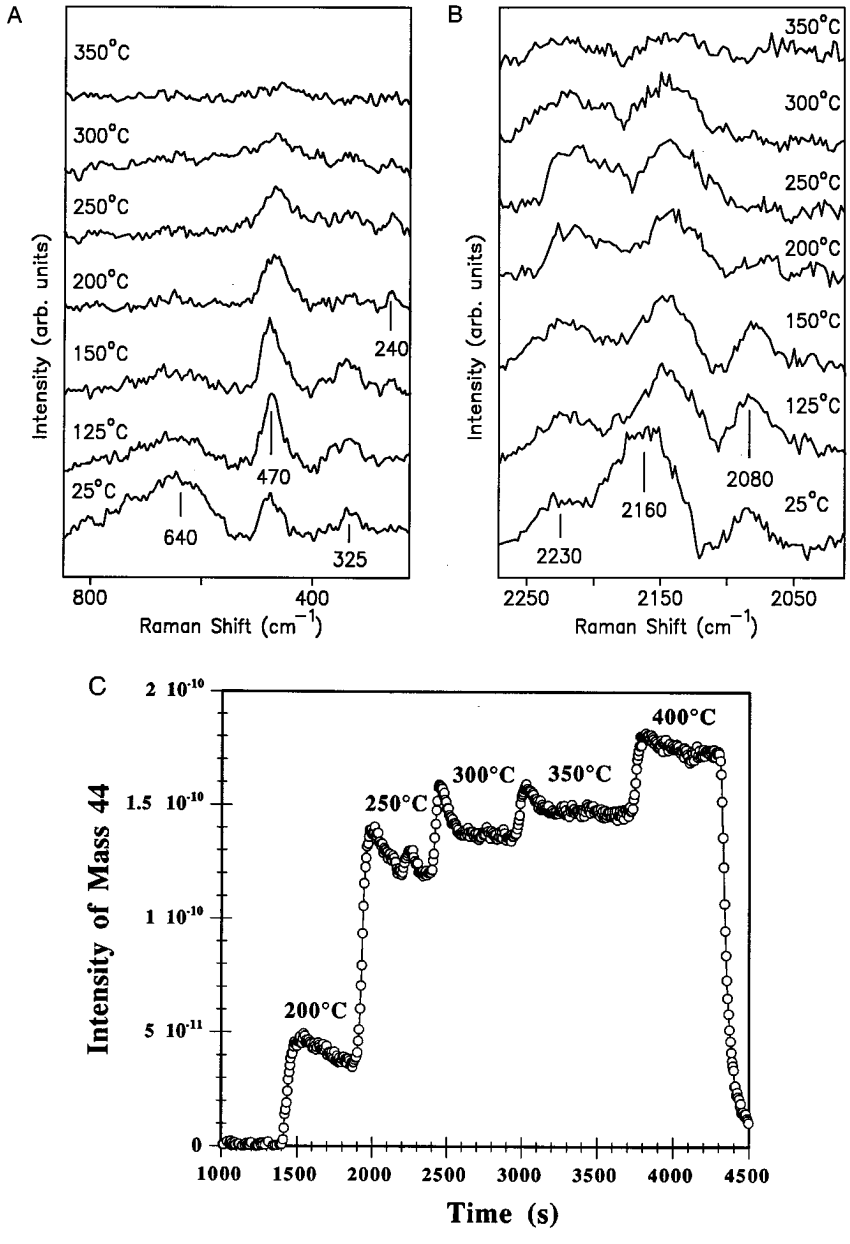

FIG. 5. Simultaneous SERS and mass spectrometric measurements obtained during reaction of 100 cm^3 min^{-1} of 50% NO and 50% CO on Pt: (A) Temperature-dependent SER spectra in the low-frequency region obtained with 20 s integration time; (B) Temperature-dependent SER spectra in the high-frequency region obtained with 60 s integration time; (C) Intensity of mass 44 vs time.

containing a fourfold excess of either CO or NO. Vibrational features essentially similar to those observed under equimolar conditions were also detected in those cases, with SERS bands arising from both NO and CO adsorption being evident at room temperature. Reaction rates, as detected by the increase in mass 44 intensity, were found to be considerably (ca threefold) lower than those for the equimolar ratio. Kinetics experiments utilizing ^{13}CO failed to detect any N_2O formation, perhaps due to the lower overall rates and hence weaker MS signals under these reaction conditions.

As already mentioned, a more cursory examination of the present system was also undertaken by means of infrared reflection–absorption spectroscopy (IRAS). While IRAS lacks the surface sensitivity and wide frequency range attainable by SERS, the former can yield surface vibrational information that is a useful complement to the latter data. This is partly because the infrared absorbances can provide semi-quantitative estimates of adsorbate coverages, since the IRAS responses should be free from any "special surface-site" requirements that may affect the SER spectra. The samples used for these experiments were identical

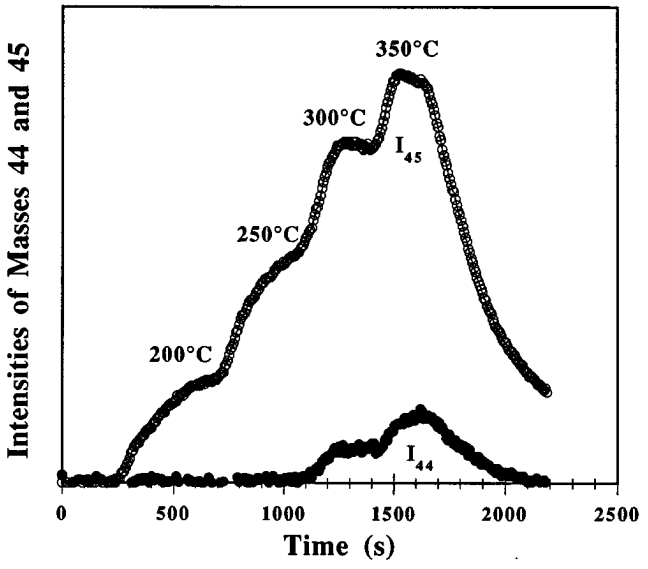

FIG. 6. Isotopic kinetic experiment utilizing a flow of 20 cm^3 min^{-1} of 50% ^{13}CO and 50% NO at 1 atm. The temperature profile and the intensities of masses 44 and 45 are presented as a function of time.

to those utilized in the SERS experiments, except that they had a larger (1 cm^2) surface area, obliged by the usual optical requirements of IRAS. Substantial gas-phase interference, coupled with the low surface area of the catalyst, precluded collection of atmospheric-pressure data, but it was possible to obtain acceptable-quality surface signals when using reactant pressures up to about 5 Torr. The best signals, however, were obtained when the gas-phase reactants were purged from the reactor prior to spectral acquisition. While such a procedure is obviously not convenient for obtaining temperature-dependent spectral sequences, it is useful for examining atmospheric-pressure adsorption at ambient temperatures. This tactic was therefore used to probe individual and co-adsorption of CO and NO at ambient temperatures.

An example of such data is presented in Fig. 7; this consists of an infrared spectrum for a Pt thin film obtained after exposure to one atmosphere of an equimolar mixture of CO and NO. Along with the C–O stretch evident at 2080 cm^{-1} is a peak at 2145 cm^{-1}; both these features are similar to those observed by using SERS (Fig. 5B). Similar experiments involving exposure to the different reactant ratios (excess NO and excess CO) at 25°C also resulted in spectra qualitatively similar to those observed with SERS. Unfortunately, it was not possible in these preliminary experiments to observe the N–O stretch, due largely to the excessive spectral background in the 1700–1900 cm^{-1} region arising from gas-phase water. However, exposing a CO-presaturated surface to NO resulted in the removal of the infrared band for adsorbed CO, a result concurring with the SERS data in Fig. 4.

Palladium Films

Similar to platinum thin films, initial spectral examination of the palladium overlayers often revealed a strong SERS feature located at 300 cm^{-1} associated with a Pd–Cl species remaining from the deposition process. Samples exhibiting this feature were pretreated at 100°C in 100 cm^3 min^{-1} of H_2 for ca 5 min, which yielded a clean background in the 200–1000 cm^{-1} region. Features associated with carbonaceous impurities (1300–1600 cm^{-1}) were also observed but were not removed by high-temperature oxidation (*vide supra*).

Following the protocol already outlined, before studying the Pd surface under reaction conditions, the temperature-dependent adsorption of each reactant was investigated separately by utilizing SERS. Figure 8A shows a typical temperature-dependent spectral sequence in the low-frequency region for a Pd film exposed to 100 cm^3 min^{-1} of NO at 1 atm, with the experimental procedure the same as detailed above. The adsorption of NO at room temperature (bottom spectra) yields an intense SERS feature at 310 cm^{-1} (with a shoulder at 285 cm^{-1}) and a broader band at 570 cm^{-1}. Unlike platinum, no spectral features were observed in the 2100–2300 cm^{-1} range. Upon heating to 100°C, the intensity of the 310 and 570 cm^{-1} features decreased and the overlapping band at 285 cm^{-1} became more prevalent. Raising the temperature to 150°C induced the disappearance of the 310 cm^{-1} feature and the severe attenuation of the 285 cm^{-1} band, along with the appearance of a peak at 245 cm^{-1}. The 570 cm^{-1} feature was also removed by this temperature. Further heating of the sample to 200°C caused the removal of the 285 cm^{-1} band, but without much change in the intensity of the 245 cm^{-1} feature. Additionally, two weak, broad bands were observed at 450 and 665 cm^{-1} (Fig. 8A). Raising the temperature further resulted in the removal of the 245 cm^{-1} band and a growth in the intensity of the 450 and 665 cm^{-1} features.

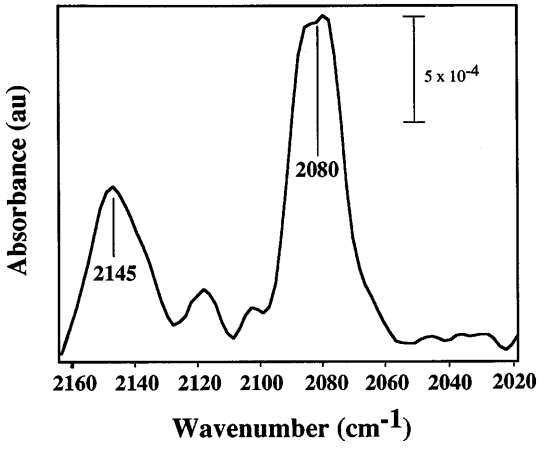

FIG. 7. Infrared absorption spectrum of 50% NO and 50% CO adsorbed on a Pt film.

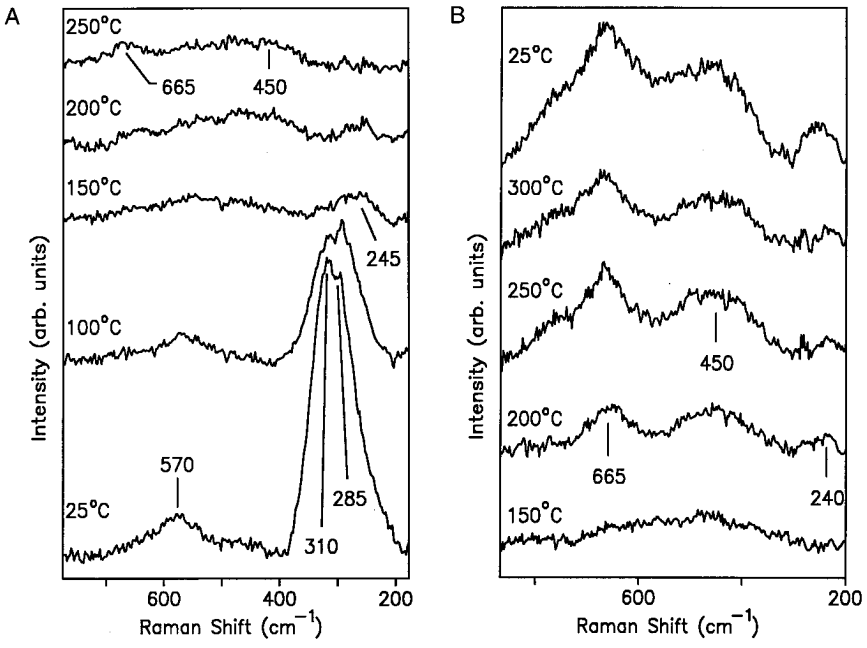

FIG. 8. Temperature-dependent SER spectra for a Pd surface exposed to: (A) 100 cm^3 min^{-1} of NO at 1 atm and 20 s spectral integration time; (B) 100 cm^3 min^{-1} of O_2 at 1 atm and 20 s spectral integration time.

In order to help diagnose which features formed during NO adsorption (Fig. 8A) may be associated with palladium oxide, a Pd surface was heated in pure O_2 at 100 cm^3 min^{-1} at 1 atm. Typical temperature-dependent SER spectra resulting from this procedure are presented in Fig. 8B. No spectral changes were observed until the sample was heated to 200°C, where three features located at 240, ca 450 and 665 cm^{-1} appeared. Upon further heating to 250°C both the broad ca 450 and sharp 665 cm^{-1} features grew, while the 240 cm^{-1} band was attenuated. Further heating of the sample resulted in little change in the SER spectral intensities. On cooling the sample to 25°C, all three bands were present. These results contrast with those obtained for platinum, where heating in pure oxygen under similar conditions yielded no SERS features.

As for Pt, assignment of these features is not straightforward and is discussed below. In order to aid the reader's appreciation of the spectral results, however, we again mention some assignments in advance. The 310 cm^{-1} band is assigned to the Pd–NO stretch of bridge-bound NO, while the 285 cm^{-1} feature is attributed to the Pt–N stretch of adsorbed atomic nitrogen and is apparently similar to the 295 cm^{-1} band observed on Pt at higher temperatures (*vide supra*). The 245 cm^{-1} feature is attributed to the Pd–O stretch of a PdO_x moiety.

Typical temperature-dependent SER spectra arising from CO adsorption on palladium are shown in Figs. 9A and B, again referring to low- and high-frequency segments, respectively. The surface was exposed to 100 cm^3 min^{-1} of pure CO at room temperature (bottom spectra) and then subsequently heated. In the low-frequency region a band was observed at 360 cm^{-1} along with a weak shoulder at ca 470 cm^{-1}. Two bands at 1960 and 2060 cm^{-1} are also evident in the high-frequency region. Raising the sample temperature to 100°C resulted in the removal of the features at 470 and 2060 cm^{-1}, while the intensity of the other bands decreased slightly. Upon further heating the latter bands were markedly attenuated, however, being removed by ca 200°C. Carbon monoxide adsorption has been studied extensively on both polycrystalline (57) and single-crystal (58) Pd surfaces. Based on these studies, we assign the 360 and 1960 cm^{-1} bands to the Pd–C and CO stretching modes of CO bound to twofold bridging sites, with the 470 and 2060 cm^{-1} features being attributed to the Pt–C and CO stretching vibrations of terminally bound CO.

Since both NO and CO adsorption again produced strong SERS features on palladium, experiments involving sequential dosing of reactants were performed to determine the nature of competitive adsorption. The protocol was identical to that utilized for platinum (*vide supra*). It was observed that NO displaced CO from a palladium surface, as adjudged by the disappearance of adsorbed CO features and their replacement by bands associated with NO adsorption. The converse procedure indicated that CO could not replace NO. Interestingly, both these results are identical to those obtained for platinum.

To gain further insight into the competitive adsorption of these gases, the following transient experiment was

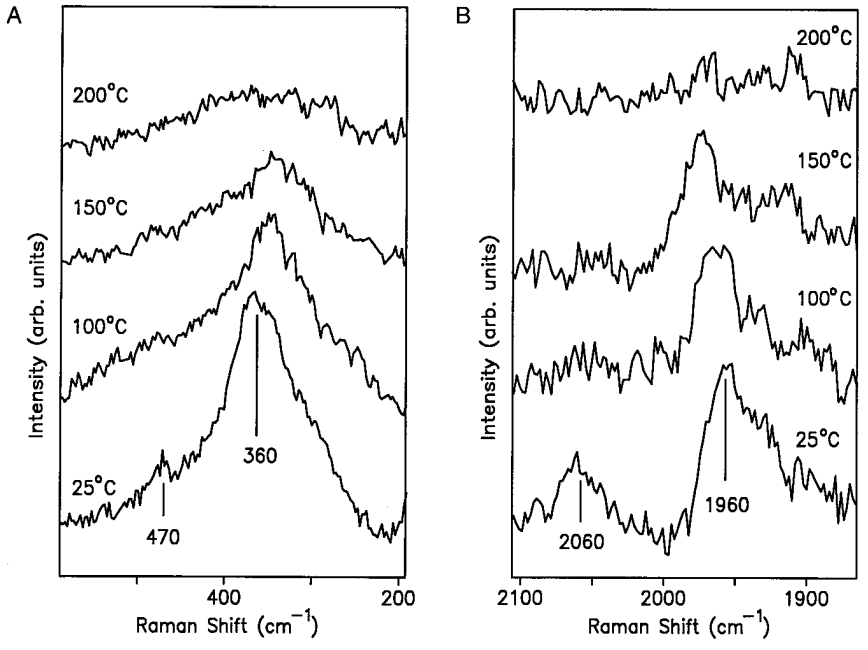

FIG. 9. Temperature-dependent SER spectrum of a Pd surface exposed to 100 cm^3 min^{-1} of CO at 1 atm: (A) Low frequency spectra obtained with 20 s integration time; (B) High frequency spectra obtained with 60 s integration time.

performed (Figs. 10A, B). A Pd surface was exposed to 50 cm^3 min^{-1} of pure CO at 1 atm and 25°C until no further spectral changes were observed. At t = 0 s, 50 cm^3 min^{-1} of NO was added to the gas flow, so as to produce an equimolar CO/NO mixture, and SER spectra were obtained every 20 s (note that the time values indicated above each spectrum refer to the lapse between the addition of NO and the end of each 10-s spectral acquisition period). The strong band at 360 cm^{-1}, indicative of CO adsorption, is seen to be slowly replaced (over ca 4 min) by the strong NO-associated

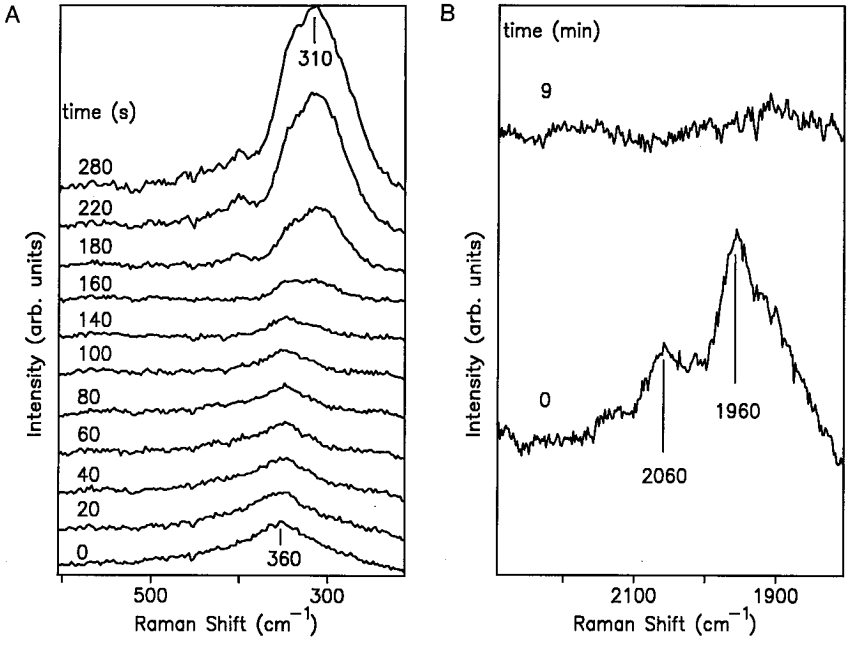

FIG. 10. (A) Time-dependent SER spectra of a Pd surface initially exposed to 50 cm^3 min^{-1} of CO, followed by addition of 50 cm^3 min^{-1} of NO to the flow at t = 0 s at 1 atm and 25°C. Spectral integration time was 20 s. (B) High-frequency region of SER spectra obtained with 60 s integration time before and 9 min after addition of NO to CO.

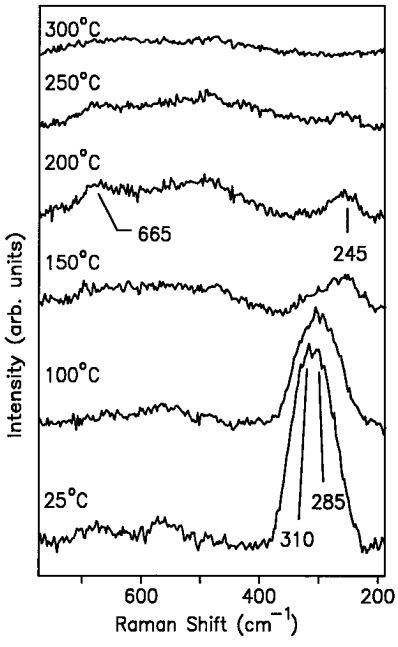

FIG. 11. Temperature-dependent SER spectra obtained during reaction of 100 cm^3 min^{-1} of 50% NO and 50% CO on Pd at 1 atm.

310 cm^{-1} feature (Fig. 10A). Further evidence of the displacement of CO is seen in the high-frequency spectra before and 9 min after addition of NO (Fig. 10B), which reveals the two bands at 1965 and 2080 cm^{-1} being completely removed. These results show that NO can displace CO even when the latter is given the advantage of continued presence in the gas phase as well as prior adsorption.

As with platinum, the reaction utilizing an equimolar NO/CO mixture was studied on Pd with SERS and MS. Figure 11 shows a typical temperature-dependent SER spectral sequence for a Pd surface heated in an equimolar mixture of NO and CO, with 50 cm^3 min^{-1} of each at 1 atm. At room temperature (bottom spectrum) the strong feature at 310 cm^{-1} observed during NO adsorption (Fig. 8A) is present, along with an overlapping band at 285 cm^{-1}. Heating the surface to 100°C resulted in the diminution of the 310 cm^{-1} band. Further heating to 150°C caused severe attenuation of these features along with the appearance of a band at 245 cm^{-1}. Bands at 665 and ca 450 cm^{-1} appeared upon heating to 200°C, while the 245 cm^{-1} peak remained unchanged and the 285 cm^{-1} feature was completely removed. Subsequent heating caused the removal of all remaining bands by 300°C. It is interesting that the observed spectral behavior mirrors closely that of pure NO, except for the absence of a strong 570 cm^{-1} band at room temperature. As might be expected from the results of the competitive adsorption experiment (Figs. 10A, B), no features associated with adsorbed CO were discernable under these conditions. This is in contrast to the corresponding results for Pt (Figs. 5A, B). Also differing from platinum, no features were observed in the 2100–2300 cm^{-1} region.

Mass spectral measurements carried out under conditions of equimolar reactants revealed an onset of detectable reaction at 200°C, as evidenced by an increase in the mass 44 intensity. Experiments involving an equimolar mixture of ^{13}CO and NO indicated that only CO_2 was being formed, as evidenced by the appearance of only mass 45. The temperature-dependent production of CO_2 increased in a manner similar to that observed for platinum (Fig. 5C), with the overall change in mass 44 intensity (i.e., CO_2 partial pressure) indicating that the rates of reaction were similar on both metals.

Unfortunately, the N–O stretching vibration for terminal (1660–1800 cm^{-1}) and bridged (1400–1620 cm^{-1}) NO was not observed on either Pt or Pd in this study. Similarly, we were also unable to observe internal NO stretching modes in our recent investigations of NO reduction on Rh (23, 52). This was probably because of a low Raman scattering cross section and interference from background features associated with carbonaceous impurities (*vide supra*). Indeed, the internal N–O stretching vibration has only recently been observed with SERS during an electrochemical study involving NO adsorption on iridium (59). While this latter case represented an optimal environment for the observation of the N–O stretch, due partly to its relatively high frequency (ca 1820 cm^{-1}) under these conditions, the band was weak in comparison with the analogous infrared spectra.

DISCUSSION

Identity of NO-related SERS Features

Before discussing the assignments of NO-related features on both Pt and Pd, it is useful to review our earlier findings regarding NO adsorption on rhodium (23). A single SERS feature at 315 cm^{-1} was induced at room temperature by NO adsorption on Rh, which grew in intensity as the sample was heated, yet was attenuated beyond 300°C. This band was attributed to the Rh–N stretch of adsorbed atomic nitrogen, based partly on this temperature-dependent behavior (cf. Ref. (47)). Additionally, the surface was oxidized extensively at higher temperatures (>300°C) in a manner similar to that reported elsewhere (51). These observations indicate the occurrence of extensive NO dissociation on rhodium, even at room temperature. Based on literature reports for NO adsorption of both Pt (1–11) and Pd (12–22), one would expect significantly less dissociation than that observed for Rh. The present study shows that the temperature-dependent SER spectra of NO adsorption on Pt (Fig. 1) and Pd (Fig. 8A) at 1 atm are distinctly different than for Rh. Keeping in mind the possible origins of these features (such as NO, N, O), we now proceed with assigning the corresponding SERS bands observed on Pt and Pd.

As detailed above, exposing a reduced Pt surface to NO at room temperature yielded several Raman features (Figs. 1A, B). While we assigned the 325 cm^{-1} band in an earlier report tentatively to the Pt–N stretch of adsorbed atomic nitrogen (52), that study lacked information on its temperature-dependent behavior. The attenuation of the band with increasing temperature as observed here (Fig. 1A) is not suggestive of a dissociation process, especially since the removal temperature (ca 100–150°C) is well below reported N_2 desorption temperatures from Pt (1, 3, 7). It therefore seems more likely that this vibration arises from molecularly adsorbed NO.

Further insight into the nature of the species responsible for this vibrational feature is gleaned from literature EELS data obtained during NO adsorption on Pt single crystals. Ibach and Lewald (2) observed bands at 310 and 1510 cm^{-1} at low coverages during NO adsorption on Pt(111). This bridging NO was observed to desorb by 150°C, the same temperature at which the present 325 cm^{-1} band is attenuated. Similarly, Gland and Sexton (3) encountered 350 and 1470 cm^{-1} bands for dilute NO adlayers, which were attributed to bridge-bound NO; this desorbed by ca 100°C. These findings, therefore, support the assignment of the 325 cm^{-1} band observed here (Fig. 1A) to the Pt–NO stretch of molecular NO possibly adsorbed on bridging sites.

By examining the temperature dependence of the 240 and 470 cm^{-1} features (Fig. 1A), it is apparent that the growth and eventual disappearance of these bands occur in tandem. Similarly related NO vibrations on Pt(111) have been observed with EELS by Gland and Sexton (3), who recorded three peaks at high NO coverages (290, 450, and 1710 cm^{-1}) associated with terminally bound NO. Pirug *et al*. (9) have also assigned low frequency bands observed at 230 and 380 cm^{-1} upon dosing NO at 25°C on Pt(100) to Pt–NO stretching and Pt–N–O bending modes, respectively, of terminal NO. These results, combined with vibrational spectra of nitrosyl complexes (60), lead us to assign the 240 and 475 cm^{-1} features (Fig. 1A) to Pt–NO stretching and Pt–N–O bending vibrations of terminally bound NO. The weak 295 cm^{-1} feature that appears as the 240 cm^{-1} band attenuates at ca 200°C is probably not associated with a different form of molecular NO, since TPD studies (1–6, 11) have indicated that NO desorbs from Pt by this temperature. Since desorptive nitrogen recombination has commonly been observed at higher temperatures (1, 3, 4) and this 295 cm^{-1} band is attenuated by 300°C, we tentatively assign this vibration to the Pt–N stretch of adsorbed atomic nitrogen.

The high-frequency bands observed here on Pt at ca 2180 and 2250 cm^{-1} during exposure to NO (Fig. 1B) have not been reported in other vibrational studies. However, several infrared spectral reports of the NO–CO reaction on supported Pt have noted the occurrence of apparently similar bands (35, 61–64). The ca 2250 cm^{-1} feature is commonly attributed to an adsorbed isocyanate species (–NCO) (35, 61–64), while the 2180 cm^{-1} band is assigned to either adsorbed cyanide (35) or isocyanate anion (60, 61). Both these species are known to be formed by reaction of CO with NO or its dissociation products, yet there is uncertainty regarding the location of these adsorbates with respect to the metal and support. In addition to supported catalysts, similar bands have been observed on polycrystalline (65) and single-crystal Pt (4). This evidence suggests that the 2250 cm^{-1} band observed in the present study (Fig. 1B) probably arises from an asymmetric stretching mode of adsorbed isocyanate. The formation of this species during NO exposure, even in the absence of CO, indicates that NO, or its dissociation products, reacts with surface carbonaceous impurities. While the precise nature of the species giving rise to the 2180 cm^{-1} feature is not as clear (either adsorbed cyanate ion or cyanide), it also appears to arise from reaction between adsorbed NO and carbonaceous impurities.

The assignment of the band at ca 610 cm^{-1} is not immediately evident. One possibility is the N–C–O symmetric stretching mode of adsorbed isocyanate, which has been reported in an EELS study of HNCO adsorption on Pt(111) (4). However, the lack of correlation between the temperature-dependent behavior of the 2250 cm^{-1} feature with the ca 610 cm^{-1} band casts doubt on this option. A more likely possibility is a surface carbonate formed through reaction between carbonaceous impurities and adsorbed atomic oxygen formed by NO dissociation. The presence of such a carbonate species during reaction conditions on supported Pt has been reported by Matyshak *et al*. [64]. Lending credence to this assertion is our observation of a similar band when either Rh or Pt surfaces were heated in CO/O_2 mixtures.

Nitric oxide adsorption on Pd surfaces yielded less complex spectra than for Pt, most notable being the absence of higher-frequency bands attributable to cyanate-like moieties. However, the room-temperature spectra (Fig. 8A) reveals several low-frequency vibrations associated with NO and its dissociation products. The attenuation of the 310 cm^{-1} band upon heating to 150°C is identical to the behavior of the 325 cm^{-1} NO band on platinum, suggesting that these features arise from similar species. Indeed, an EELS study (13) of NO on Pd(100) reported a 310 cm^{-1} band at low coverage which was assigned to the Pd–NO stretch of bridged NO. The 285 cm^{-1} feature, seen in Fig. 8A as a shoulder at room temperature and more clearly by 100°C, is completely attenuated only at 200°C. This indicates that the species is more strongly adsorbed than the 310 cm^{-1} NO feature. The presence of adsorbed atomic oxygen (*vide infra*) also suggests that there is significant NO dissociation at room temperature. It is therefore likely that this 285 cm^{-1} vibration arises from the Pd–N stretch of adsorbed atomic nitrogen, similar to the 295 cm^{-1} feature observed on Pt at higher temperatures (*vide supra*).

However, it is possible that this feature arises from a different state of adsorbed NO.

The 570 cm^{-1} band observed at room temperature (Fig. 8B) is similar to an EELS feature at 500–525 cm^{-1} that Ramsier *et al*. (20) reported when NO dissociated at around 200°C on both Pd(111) and Pd(112). This energy loss was assigned to the Pd–O stretch of adsorbed atomic oxygen. While adsorption of oxygen at room temperature yielded no such SERS feature in this study, it has been reported (15) that NO adsorbed on Pd(111) can produce higher coverages of atomic oxygen than arise from dissociation of O_2 at 25°C. Furthermore, the 570 cm^{-1} band appears to be absent in the presence of CO (Fig. 11), indicating possible reactive removal (39, 66). We therefore assign this feature to the Pd–O stretch of adsorbed atomic oxygen. The 665 and ca 450 cm^{-1} bands observed above 150°C (Fig. 8A) are similar to those observed during thermal O_2 oxidation of Pd (Fig. 8B), and are assigned to internal vibrations of a PdO_x moiety. In a related work, Weber *et al*. (67) investigated oxidized Pd with Raman spectroscopy and observed a strong band at 650 cm^{-1} and weaker bands at 278, 423, 445, and 571 cm^{-1}. The 245 cm^{-1} feature observed at higher temperatures during NO adsorption on Pd also appears at similar temperatures during palladium oxidation (Fig. 8B). However, the temperature-dependent nature of this band (Fig. 8B) indicates that it is a behaviorally distinct oxide. This is similar to the thermal oxidation of Rh (51), where two distinct oxides were detected at higher temperatures.

Extent of NO Dissociation

Ascertaining the extent of NO dissociation on the catalyst is important because it affects both the reaction pathway as well as kinetics. As will be discussed later, this issue is central in explaining differences between Pt and Pd as catalysts for the CO–NO reaction. Several studies have indicated that NO dissociates to a modest extent on both surfaces. At lower temperatures, only a small degree of dissociation has been detected on Pt(111) (2–6) and Pt(110) (4, 7), while Pt(100) appears to be the most active low-index face (4). Polycrystalline (9–11) as well as supported (62) Pt have also been shown to exhibit some activity towards NO dissociation (10–15%) at elevated temperatures. On palladium, low levels of NO dissociation have been reported for the (111) (14, 16, 20), (110) (14), (100) (12, 14), and (112) (20) faces, in addition to significant dissociation at higher temperatures (>200°C) on polycrystalline surfaces (21, 22).

Our results appear consistent with these findings. We have found rhodium to be especially active with regards to NO dissociation (23), with more extensive dissociation detected than for either platinum or palladium. However, Pd does appear to be more active than Pt in this regard. While molecularly adsorbed NO is the dominant surface species on Pt below 250°C, the presence of carbonate and isocyanate species suggests that some dissociation occurs even at room temperature (Figs. 1A, B). Further, the observance of significant amounts of N_2O formation during reaction over Pt at higher temperatures implies that significant dissociation is occurring, as adsorbed nitrogen is necessary for this product to form (*vide infra*). The presence of atomic oxygen and possibly nitrogen on Pd at room temperature indicates that dissociation has occurred (Fig. 8A), probably to a greater extent than on Pt. The formation of palladium oxide at higher temperatures provides a further indication that significant quantities of atomic oxygen are being produced by NO adsorption on Pd (Fig. 8A). As highly stepped or kinked surfaces have been shown to be more active for NO dissociation (20, 24), it is not surprising that significant NO decomposition is occurring on the roughened substrates utilized here.

Implications for the NO–CO Reaction Mechanism

Having discerned that both platinum and palladium dissociate NO to a certain extent, it is desirable to determine the role that this process plays in determining the reaction pathway and selectivity. As we shall see below, the marked differences between the NO decomposition activity of these metals is consistent with the general notion that Rh is a better catalyst for NO reduction than Pt or Pd because of its greater ability to dissociate NO. Specifically, the observed selectivities towards CO_2 and/or N_2O can be, in part, rationalized by the surface speciation detected under reaction conditions.

The commonly accepted reaction mechanism for NO reduction by CO over transition metals involves adsorption of reactants, dissociation of NO, and subsequent surface reactions to form N_2, N_2O, and CO_2. Generally, either NO dissociation [1] or a bimolecular reaction between CO and NO [2]:

$$NO_{(ads)} + S \Rightarrow N_{(ads)} + O_{(ads)} \quad [1]$$

$$NO_{(ads)} + CO_{(ads)} \Rightarrow CO_2 + N_{(ads)} + S \quad [2]$$

are thought to be rate limiting (S denotes a surface site). It has been suggested by several investigators that the NO dissociation reaction [1] is rate determining on supported (34) as well as polycrystalline (35) Pt, while more recent kinetic (37) and spectroscopic (38) studies on polycrystalline Pt have pointed to the bimolecular step [2] as being rate limiting. There is also much debate on which step is rate determining on Pd. Support for the bimolecular RDS can be found in studies on single crystal (39, 40), polycrystalline (41), and supported (42) Pd. In contrast, Moriki *et al*. (36) have proposed that NO dissociation is rate limiting for reaction over polycrystalline Pd. As these studies were conducted over a wide range of pressures (from UHV up to 1 Torr), the RDS for this reaction appears to be distinctly pressure-sensitive. Additionally, the temperature of reaction can influence the RDS, since processes such as NO

dissociation and surface oxidation are more facile at higher temperatures (*vide infra*). Unland (60, 61) has also suggested that the formation of isocyanate species by the combination of adsorbed atomic nitrogen and CO may be an important step. However while isocyanate is a commonly observed surface species, it is not generally considered to be a significant intermediate (35). Indeed, lack of a frequency shift in the observed isocyanate vibrations during transient ^{13}CO isotope experiments over Pt in the present study precludes this possibility.

Unlike the CO–NO reaction on Rh (23), where CO_2 and N_2 were found to be the only products, reaction on Pt under conditions of equimolar gas flow resulted in formation of both N_2O and CO_2 (Fig. 6). Therefore it is particularly interesting in this case to see if correlations can be made between catalyst selectivity and behavior of the surface species. While NO can displace CO from a CO-saturated surface (Fig. 4), both reactants adsorb to a comparable extent on Pt over a wide range of reaction conditions if they are simultaneously present in the gas-phase (Figs. 5A, B). Between 150°C and 200°C, the amount of CO on the surface decreased, as evidenced by a reduction in the intensity of the 2080 cm^{-1} feature (Fig. 5B). It is unlikely that this is due to desorption, which would not be anticipated until higher temperatures (>350°C) at this pressure (68). Furthermore, isocyanate formation from CO can also be ruled out as a reason for these observations, based on the absence of $N^{13}CO$ formation when ^{13}CO was used. Thus, the most probable explanation for CO removal from the surface lies in its reaction with adsorbed atomic oxygen from NO dissociation or with adsorbed NO in a bimolecular reaction step. The simultaneous mass spectrometric measurements (Fig. 5C) show the first detectable appearance of the mass 44 peak at 200°C, the temperature corresponding to the disappearance of adsorbed CO and decrease in the amount of terminally-bound NO (240 and 470 cm^{-1}). In addition, the ^{13}CO isotope experiment under the same conditions (Fig. 6) reveals that CO_2 is the only product at this temperature. Such a correlation between the behavior of surface and gas-phase species indicates that CO is being reactively removed from the surface. However, it is difficult to say which, if not both, of the above reaction pathways might be predominant in the formation of CO_2, since either appears consistent with the observed product formation.

It is also desirable to similarly link the behavior of adsorbed NO to the onset of reaction. It is clear that the adsorbed NO molecules evidenced by the 240 and 470 cm^{-1} features remain on the surface as high as 250°C but are seen to decrease upon further heating (Fig. 5A). The equimolar ^{13}CO isotope experiment (Fig. 6) shows the onset of detectable N_2O production at these temperatures, indicating that there is some contribution from this product in the mass 44 peak observed by simultaneous mass spectrometric measurements (Fig. 5C). Thus, the decrease in the surface concentration of these species at 300°C may be at least partly rationalized, based on their removal via N_2O formation.

In contrast with the product distribution observed for platinum, CO_2 was found to be the only detectable product during reaction over Pd (*vide supra*). Examining the species present on the surface during the reaction (Fig. 11) provides some insight into this process. As might be expected, based on the transient replacement of adsorbed CO by addition of gas phase NO (Figs. 10A, B), CO adsorption is effectively blocked at all temperatures by NO and its dissociation products. While this observation is different than that observed for Pt above, it is very similar to the absence of adsorbed CO observed during reaction over Rh (23). At the onset of detectable reaction (200°C), molecular NO (310 cm^{-1}) has been removed and the surface is dominated by PdO_x species (670, ca 450 and 245 cm^{-1}). As N_2O formation necessarily requires the presence of adsorbed NO and atomic nitrogen at adjacent sites, oxidation of the surface may hamper this process at these temperatures. The removal of oxide features by ca 300°C (Fig. 11) is a clear indication that CO is reactively removing oxygen, as this moiety has been observed to desorb from palladium surfaces at much higher temperatures (Fig. 8B; Ref. (65)). Therefore, the reaction between adsorbed CO and atomic oxygen is occurring fast enough that the oxygen supply on the surface is severely depleted. This dissipation of surface oxygen may indicate that NO dissociation is rate-limiting at these temperatures.

The fact that Pt shows some selectivity towards N_2O at higher temperatures, while Rh and Pd do not, appears to be related to their relative abilities to dissociate NO. While N_2O formation would be facilitated by the availability of substantial quantities of molecular NO on Pt, it would be hampered at lower temperatures by limited atomic nitrogen, thus resulting in detectable production only at higher temperatures. Rhodium and palladium, on the other hand, favored NO dissociation more strongly, which led to a completely nitrogen and oxygen covered surface at higher temperatures that most likely hampered N_2O formation in both cases. Similarly, a recent report (69) involving this reaction over Rh (111) and (100) at relatively high pressures (100 Torr) suggests that N_2O selectivity decreases as the extent of NO dissociation increases.

CONCLUDING REMARKS

Surface-enhanced Raman spectroscopy, combined with mass spectrometry, has been employed to investigate NO reduction by CO over platinum and palladium under catalytically relevant conditions. There are several similarities and differences between the behavior of surface moiety during both reactant adsorption and reaction. During NO adsorption, molecular NO dominated both surfaces at lower temperatures, with a small degree of dissociation observed

for each metal. However, while NO and its dissociation products effectively blocked adsorption of CO during reaction over Pd, significant quantities of adsorbed CO were detected on Pt under similar conditions. While CO_2 and N_2 were the only products observed during reaction over Pd, N_2O formation was detected at higher temperatures for Pt. These findings, coupled with our previous observations during the NO–CO reaction on Rh, suggest that the higher the ability to dissociate NO, the lower the selectivity toward N_2O for these metals, at atmospheric pressure.

ACKNOWLEDGMENT

This work is supported by a grant to CGT and MJW (CTS-9312008) from the National Science Foundation.

REFERENCES

1. Comrie, C. M., Weinberg, W. H., and Lambert, R. M., *Surf. Sci.* **57**, 619 (1976).
2. Ibach, H., and Lehwald, S., *Surf. Sci.* **76**, 1 (1978).
3. Gland, J. L., and Sexton, B. A., *Surf. Sci.* **94**, 355 (1980).
4. Gorte, R. J., Schmidt, L. D., and Gland, J. L., *Surf. Sci.* **109**, 367 (1981).
5. Campbell, C. T., Ertl, G., and Segner, J., *Surf. Sci.* **115**, 309 (1982).
6. Hayden, B. E., *Surf. Sci.* **131**, 419 (1983).
7. Gorte, R. J., and Gland, J. L., *Surf. Sci.* **102**, 348 (1981).
8. Bonzel, H. P., and Pirug, G., *Surf. Sci.* **62**, 45 (1977).
9. Pirug, G., Bonzel, H. P., Hopster, H., and Ibach, H., *J. Chem. Phys.* **71**, 93 (1979).
10. Mummey, M. J., and Schmidt, L. D., *Surf. Sci.* **109**, 29 (1981).
11. Wickham, D. T., Banse, B. A., and Koel, B. E., *Surf. Sci.* **223**, 82 (1989).
12. Jorgenson, S. W., Canning, N. D. S., and Madix, R. J., *Surf. Sci.* **179**, 332 (1987).
13. Nyberg, C., and Uvdal, P., *Surf. Sci.* **204**, 517 (1988).
14. Sugai, S., Watanabe, H., Kioka, T., Miki, H., and Kawasaki, K., *Surf. Sci.* **259**, 109 (1991).
15. Conrad, H., Ertl, G., Kuppers, J., and Latta, E. E., *Surf. Sci.* **65**, 235 (1977).
16. Schmick, H.-D., and Wassmuth, H.-W., *Surf. Sci.* **123**, 471 (1982).
17. Miyazaki, E., Kojima, I., Orita, M., Sawa, K., Sanada, N., Miyahara, T., and Kato, H., *Surf. Sci.* **176**, L841 (1986).
18. Bertolo, M., and Jacobi, K., *Surf. Sci.* **226**, 207 (1990).
19. Wickham, D. T., Banse, B. A., and Koel, B. E., *Surf. Sci.* **243**, 83 (1991).
20. Ramsier, R. D., Gao, Q., Waltenberg, H. N., and Yates, J. T., Jr., *J. Chem. Phys.* **100**, 6837 (1994).
21. Matsumoto, Y., Onishi, T., and Tamaru, K., *J. Chem. Soc. Faraday Trans. 1* **76**, 1116 (1980).
22. Miki, H., Nagase, H., Nagase, T., Kioka, T., Sugai, S., and Kawasaki, K., *Appl. Surf. Sci.* **33/34**, 292 (1988).
23. Tolia, A. A., Williams, C. T., Takoudis, C. G., and Weaver, M. J., *J. Phys. Chem.* **99**, 4599 (1995).
24. Morrow, B. A., Chevrier, J. P., and Moran, L. E., *J. Catal.* **91**, 208 (1985).
25. Lambert, R. M., and Comrie, C. M., *Surf. Sci.* **46**, 61 (1974).
26. Gorte, R. J., and Schmidt, L. D., *Surf. Sci.* **111**, 260 (1981).
27. Bonzel, H. P., and Fischer, T. F., *Surf. Sci.* **51**, 213 (1975).
28. Banholzer, W. F., and Mazel, R. I., *Surf. Sci.* **137**, 339 (1984).
29. Lesley, M. W., and Schmidt, L. D., *Chem. Phys. Lett.* **102**(5), 459 (1983).
30. Schwartz, S. B., and Schmidt, L. D., *Surf. Sci.* **183**, L269 (1987).
31. Schwartz, S. B., and Schmidt, L. D., *Surf. Sci.* **206**, 169 (1988).
32. Gardner, P., Martin, R., Tushaus, M., and Bradshaw, A. M., *Surf. Sci.* **269/270**, 405 (1992).
33. Park, Y. O., Banholzer, W. F., and Masel, R. I., *Surf. Sci.* **155**, 341 (1985).
34. Banse, B. A., Wickham, D. T., and Koel, B. E., *J. Catal.* **119**, 238 (1989).
35. Lorimer, D., and Bell, A. T., *J. Catal.* **59**, 223 (1979).
36. Moriki, S., Inoue, Y., Miyazaki, E., and Yasumori, Y., *J. Chem. Soc. Faraday Trans. 1* **78**, 171 (1982).
37. Klein, R. L., Schwartz, S., and Schmidt, L. D., *J. Phys. Chem.* **89**, 4908 (1985).
38. Scharpf, E. W., and Benziger, J. B., *J. Catal.* **136**, 342 (1992).
39. Davies, P. W., and Lambert, R. M., *Surf. Sci.* **110**, 227 (1981).
40. Yamada, T., Matsuo, I., Nakamura, J., Xie, M., Hirano, H., Matsumoto, Y., and Tanaka, K., *Surf. Sci.* **231**, 304 (1990).
41. Xi, G., Bao, J., Shao, S., and Li, S., *J. Vac. Sci. Technol. A* **10**, 2351 (1992).
42. Grill, C. M., Gonzalez, R. D., *J. Phys. Chem.* **84**, 878 (1980).
43. Butler, J. D., and Davis, D. R., *J. Chem. Soc. Dalton Trans.* **21**, 2249 (1976).
44. El Hamdaoui, A., Bergeret, G., Massardier, J., Primet, M., and Renouprez, A., *J. Catal.* **148**, 47 (1994).
45. Leung, L.-W. H., and Weaver, M. J., *J. Am. Chem. Soc.* **109**, 5113 (1987).
46. Leung, L.-W. H., and Weaver, M. J., *Langmuir* **4**, 1076 (1988).
47. Wilke, T. E., Gao, X., Takoudis, C. G., and Weaver, M. J., *Langmuir* **7**, 714 (1991).
48. Wilke, T. E., Gao, X., Takoudis, C. G., and Weaver, M. J., *J. Catal.* **130**, 62 (1991).
49. Tolia, A. A., Wilke, T. E., Weaver, M. J., and Takoudis, C. G., *Chem. Engr. Sci.* **47**, 2781 (1992).
50. Tolia, A. A., Takoudis, C. G., and Weaver, M. J., *J. Vac. Sci. Technol. A* **11**, 2013 (1993).
51. Tolia, A. A., Smiley, R., Delgass, W. N., Takoudis, C. G., and Weaver, M. J., *J. Catal.* **150**, 56 (1994).
52. Tolia, A. A., Williams, C. T., Takoudis, C. G., and Weaver, M. J., *Langmuir* **11**, 3438 (1995).
53. Gao, P., Gosztola, D., Leung, L.-W. H., and Weaver, M. J., *J. Electroanol. Chem.* **233**, 211 (1987).
54. Hoge, D., Tushaus, M., Schwiezer, E., and Bradshaw, A. M., *Chem. Phys. Lett.* **151**, 230 (1988).
55. For example, see Steininger, H., Lehwald, S., and Ibach, H., *Surf. Sci.* **123**, 264 (1982).
56. For example, see Hollins, P., and Pritchard, J., *Prog. Surf. Sci.* **19**, 275 (1985).
57. Bradshaw, A. M., and Hoffman, F. M., *Surf. Sci.* **52**, 449 (1975).
58. Bradshaw, A. M., and Hoffman, F. M., *Surf. Sci.* **72**, 513 (1978).
59. Zou, S.-Z., Gomez, R., and Weaver, M. J., in preparation.
60. For example, see Miki, E., Mizumachi, K., Ishimori, T., and Okuno, H., *Bull. Chem. Soc. Japan* **47**, 656 (1974).
61. Unland, M. L., *J. Catal.* **31**, 459 (1973).
62. Unland, M. L., *J. Phys. Chem.* **77**, 1952 (1977).
63. Solymosi, F., Sarkany, J., and Schauer, A., *J. Catal.* **46**, 297 (1977).
64. Matyshak, V. A., Gazarov, R. A., Panchishnyi, V. I., and Kadushin, A. A., *Kinet. Catal.* **29**(6), 1382 (1988).
65. Solymosi, F., and Bansagi, T., *J. Phys. Chem.* **83**, 552 (1979).
66. Stuve, E. M., Madix, R. J., and Brundle, C. R., *Surf. Sci.* **146**, 155 (1984).
67. Weber, W. H., Baird, R. J., and Graham, G. W., *J. Raman. Spec.* **19**, 239 (1988).
68. Van Slooten, R. F., and Nieuwenhuys, B. E., *J. Catal.* **122**, 429 (1990).
69. Peden, C. H. F., Belton, D. N., and Schmieg, S. J., *J. Catal.* **155**, 204 (1995).